Nanoscale

ROYAL SOCIETY OF CHEMISTRY

MINIREVIEW

View Article Online
View Journal

Check for updates

Cite this: DOI: 10.1039/d1nr03294a

Improving the performance stability of direct seawater electrolysis: from catalyst design to electrode engineering

Weiran Zheng, [a] Lawrence Yoon Suk Lee *[a,b] and Kwok-Yin Wong *[a]

Received 23rd May 2021,
Accepted 16th August 2021

DOI: 10.1039/d1nr03294a

rsc.li/nanoscale

Direct seawater electrolysis opens a new opportunity to lower the cost of hydrogen production from current water electrolysis technologies. To facilitate its commercialization, the challenges of long-term performance stability of electrochemical devices need to be first addressed and realized. This minireview summarised the common causes of performance decline during seawater electrolysis, from chemical reactions at the electrode surface to physical damage to the cell. The problems triggered by the impurities in seawater are specifically discussed. Following these issues, we further outlined the ongoing effort of counter-measurements: from electrocatalyst optimization to electrode engineering and cell design. The recent progress in selectivity tuning, surface protection, gas diffusion, and cell configuration is highlighted. In the final remark, we emphasized the need for a consensus on evaluating the stability of seawater electrolysis in the current literature.

Published on 16 August 2021. Downloaded by Hong Kong Polytechnic University on 9/9/2021 5:39:47 AM.

1. Introduction

Hydrogen fuel is widely recognized as an alternative energy source to confront the current energy crisis and climate change caused by the excessive use of carbon-based fuels. It can be easily distributed off-grid, and the combustion of hydrogen produces only water.[1] One of the most desirable methods to produce hydrogen is water electrolysis using renewable electrical energy, which is sustainable in the long term and widely accessible worldwide.[2]

Two half-reactions, hydrogen evolution reaction (HER: reactions (1) and (2)) and oxygen evolution reaction (OER: reactions (3) and (4)), are involved in water electrolysis. Depending on the pH of electrolyte, the reactions consume H^+, OH^-, and H_2O:

Cathodic:

$$H^+ + 2e^- \rightarrow H_2 \text{ (acidic)} \quad (1)$$

$$2H_2O + 2e^- \rightarrow H_2 + 2OH^- \text{(neutral or alkaline)} \quad (2)$$

Anodic:

$$2H_2O \rightarrow 4H^+ + O_2 + 4e^- \text{(acidic)} \quad (3)$$

$$4OH^- \rightarrow 2H_2O + O_2 + 4e^- \text{(alkaline)} \quad (4)$$

Currently, two mature water electrolyzers, alkaline water electrolysis (AWE) and proton exchange membrane water electrolysis (PEMWE), are commercially available, while other technologies, such as anion exchange membrane water electrolysis (AEMWE), are under development.[3] AWE requires an alkaline electrolyte, typically 25–30% KOH solution. PEMWE is performed under acidic conditions: the electrolyte is fed at the anode, and the membrane allows protons to reach the cathode for reduction. Nevertheless, both techniques demand ultra-pure water with contaminant concentration at or below the ppm level to maintain long-term operation. Typical impurities in water such as Mg^{2+}, Ca^{2+}, and Cl^- can cause cell degradation.[4,5]

The requirement for ultra-pure water increases the cost of hydrogen produced from water electrolysis and limits the deployment of water electrolysis plants in specific areas, such as arid lands and remote regions, where freshwater is considered a valuable resource. Therefore, direct electrolysis of impure water, especially the nearly unlimited seawater (96.5% of global water reserves, pH varies from 7.5 to 9.0 worldwide[6]), is a better choice to offset the cost.[7,8] Moreover, renewable electricity from wind/solar irradiation can be coupled with seawater electrolysis to produce hydrogen as an energy storage medium.[9]

In order to put direct seawater electrolysis into practice, two aspects, activity and long-term stability,[8,10] need to be addressed. Although the recently developed water-splitting catalysts have demonstrated superior activities over commercial ones in the neutral electrolyte, their long-term performance

[a]Department of Applied Biology and Chemical Technology and the State Key Laboratory of Chemical Biology and Drug Discovery, The Hong Kong Polytechnic University, Hung Hom, Kowloon, Hong Kong SAR, China.
E-mail: lawrence.ys.lee@polyu.edu.hk, kwok-yin.wong@polyu.edu.hk
[b]Research Institute for Smart Energy, The Hong Kong Polytechnic University, Hung Hom, Kowloon, Hong Kong SAR, China

Published on 16 August 2021. Downloaded by Hong Kong Polytechnic University on 9/9/2021 5:39:47 AM.

does not meet the commercial requirement (>3000 h per year for over ten years at high current density).[11] Compared with the well-defined electrolytes for AWE and PEMWE, the composition of seawater is rather complex (Table 1).[12] Multiple species co-existing in seawater pose significant challenges toward the selectivity and long-term stability of direct seawater electrolysis under the current technology of AWE and PEMWE. The causes of performance instability during seawater electrolysis (Fig. 1) will be outlined below, followed by methods currently used for addressing them: from electrocatalyst design strategies to electrode engineering.

2. How the long-term stability is evaluated?

The performance stability of water electrolysis is usually evaluated by either chronoamperometry (CA: fixed voltage between anode and cathode, monitoring the current) or chronopotentiometry (CP: fixed current, monitoring the cell voltage). During long-term electrolysis evaluated by CA, the current density declines over operation time, meaning a lower H_2 production rate. For CP, the voltage increases during electrolysis, indicating that more energy is required to maintain the desired reaction rate. Both methods can give us the energy efficiency (charge needed to generate hydrogen divided by the total charge input), but for the sake of performance-oriented hydrogen production, the CP method combined with other electrochemical techniques, such as electrochemical impedance spectroscopy (EIS), is suggested.[11]

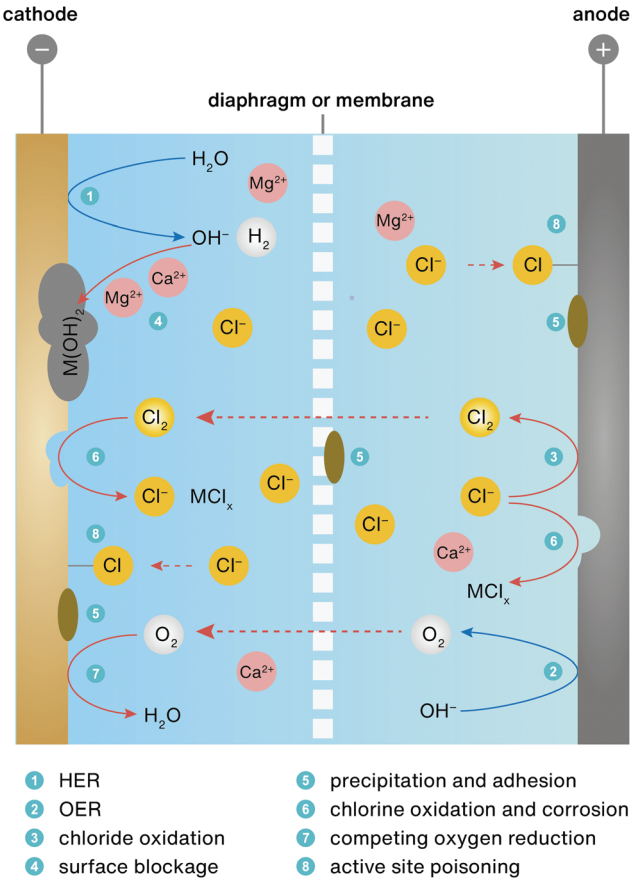

Fig. 1 Schematic overview showing the common causes of performance degradation during seawater electrolysis.

3. Causes of performance instability

Generally, the causes of instability during seawater electrolysis can be classified into chemical (*e.g.*, competing reaction, corrosion, precipitation, and surface poisoning) and physical (*e.g.*, surface blockage, adhesion, catalyst detachment/agglomeration, and surface area decrement) issues. Some problems are shared by the current AWE and PEMWE systems, while others are specifically due to seawater.

3.1. Chloride oxidation

The overall reaction rate of water electrolysis is often controlled by the sluggish OER at the anode regardless of the cell configuration. In seawater, the chloride ion is the most abundant anion species. It can be oxidized at a slightly higher potential than the OER potential (1.23 V *vs.* SHE at pH = 0 for OER).

Fig. 2A shows the Pourbaix diagram in a Cl-containing electrolyte where the OER and Cl^-/ClO^- potentials (reaction (5)) depend on the pH values while Cl_2 evolution (reaction (6)) does not. Compared with the four-electron transfer OER process, the oxidation of Cl^- involves two electrons (reactions (5) and (6)), making it kinetically more favourable over the OER at the anode during seawater electrolysis at a high current density. For example, Cl^- ions can strongly inhibit the OER on the commercial IrO_x electrocatalyst.[13] It appears that replacing the OER with a faster anodic reaction of Cl^- electrooxidation

Table 1 Common species and their concentrations in reference seawater with practical salinity of 35.000 and reference salinity of 35.16504 g kg^{-1}.[12] (concentration unit: mmol kg^{-1}, per kilogram of seawater)

Cation	Concentration	Anion	Concentration	Others	Concentration
Na^+	468.967	Cl^-	545.869	O_2	0–0.3
Mg^{2+}	52.817	SO_4^{2-}	28.235	$B(OH)_3$	0.314
Ca^{2+}	10.282	HCO_3^-	1.718	CO_2	0.010
K^+	10.208	Br^-	0.842		
Sr^{2+}	0.091	CO_3^{2-}	0.239		
		OH^-	0.008		

This journal is © The Royal Society of Chemistry 2021

Published on 16 August 2021. Downloaded by Hong Kong Polytechnic University on 9/9/2021 5:39:47 AM.

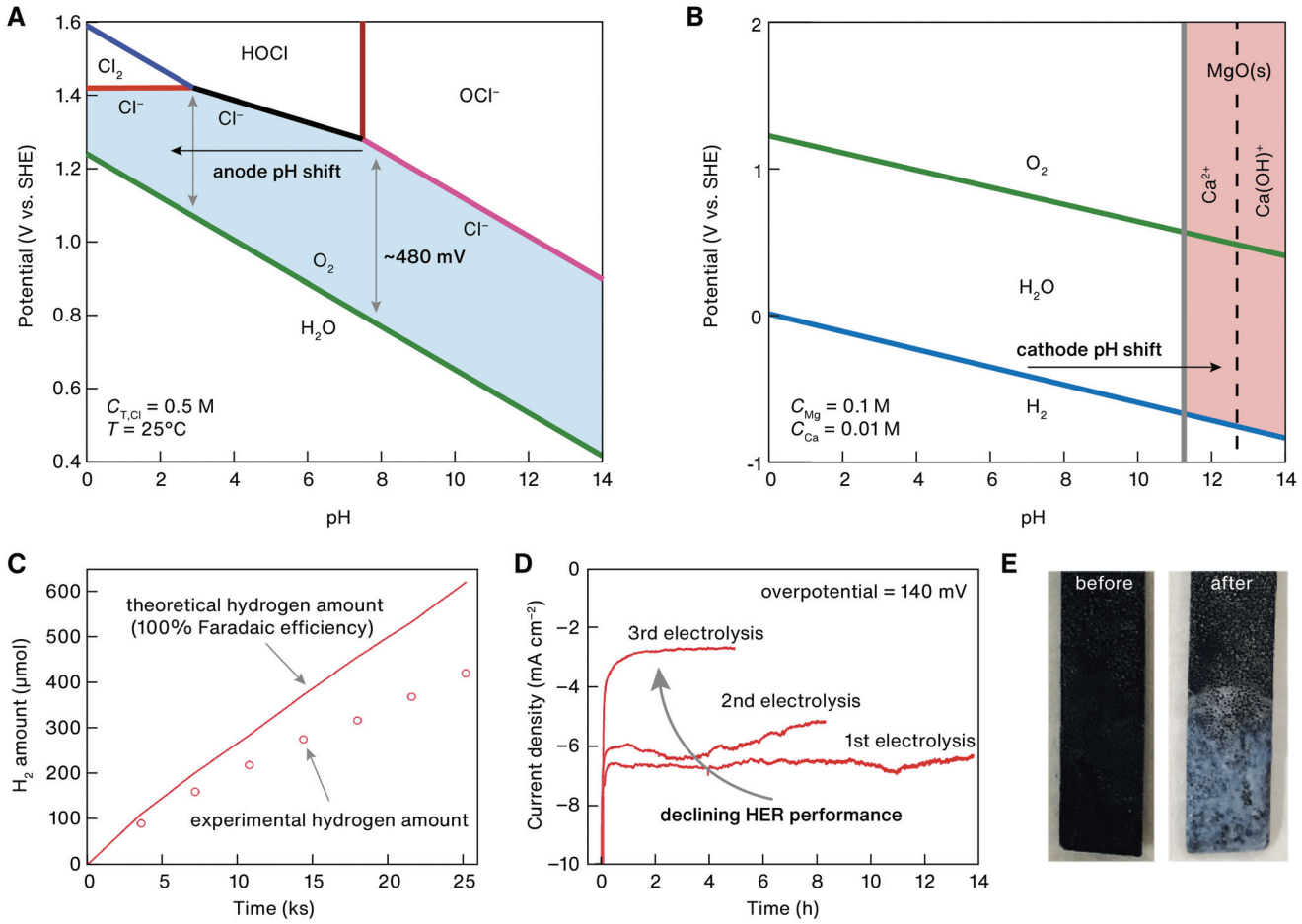

Fig. 2 (A) Pourbaix diagram showing the OER and chloride oxidation relationship in an aqueous solution containing 0.5 M total Cl species. Reprinted with permission,[19] 2016 Wiley-VCH. (B) Pourbaix diagram showing the OER in an aqueous solution containing 0.10 mM Mg^{2+} and 0.01 mM Ca^{2+} ions. Diagram predicted by materialsproject.org.[20] (C) The quantity of experimental hydrogen production compared with the theoretical hydrogen during long-term seawater electrolysis. The theoretical value was calculated based on the total charge input assuming a 100% electricity-to-hydrogen conversion. (D) HER chronoamperometric curves obtained during repeated electrolysis. The interval between each test was 24 h. (E) Photos of the electrode before and after 14 h of HER in seawater. The overpotential was 140 mV. Panels C, D, and E are reprinted with permission,[16] 2018 Royal Society of Chemistry.

can benefit the cathodic HER with accelerated hydrogen production.

Anodic:

$$\begin{aligned} &Cl^- + 2OH^- \rightarrow ClO^- + H_2O + 2e^- \\ &E^\circ = 0.89\,V\,vs.\,SHE \quad (pH = 14) \end{aligned} \tag{5}$$

$$\begin{aligned} &2Cl^- \rightarrow Cl_2 + 2e^- \\ &E^\circ = 1.36\,V\,vs.\,SHE \quad (pH = 0) \end{aligned} \tag{6}$$

However, the mass production of highly corrosive Cl_2 and ClO^- species in the electrolyzer is rather dangerous. It is well known that Cl_2 can react with most metallic materials (including stainless steel that is widely used to make electrolyzers) and some organic compounds under mild conditions.[14] Therefore, the side reaction of Cl^- electrooxidation can potentially jeopardize the structural stability of the cells and the chemical stability of electrodes and therefore should be avoided by selectively producing oxygen. In addition to Cl^-, the oxidation of Br^- ions to Br_2 occurs at 1.0873 V *vs.* SHE, which is lower than the OER potential under acidic conditions. However, since the concentration of Br^- is considerably low (0.842 mmol kg^{-1}), the impact of this reaction is negligible.

3.2. Surface blockage

Compared with the anode, the competing reactions at the cathode side are rarely mentioned since the thermodynamic reduction potentials of cations, such as Na^+, Mg^{2+}, and Ca^{2+}, are much more negative than the HER potential. Most research effort on the HER in seawater focuses on improving the catalytic activity in near-neutral pH. However, unlike laboratory testing conditions which use buffered solutions to simulate the neutral environment, natural seawater contains minor buffering species. Therefore, the local pH near both the cathode and anode during electrolysis can drift significantly.[15] Specifically, for the anode, in a neutral and unbuffered electrolyte such as seawater, the reaction consumes OH^- at low

Published on 16 August 2021. Downloaded by Hong Kong Polytechnic University on 9/9/2021 5:39:47 AM.

current densities (reaction (4)), whereby the reaction switches to H_2O oxidation at a high reaction rate (reaction (3)). Both can shift the local pH to the acidic side (Fig. 2A). For the cathode (reaction (2)), OH^- species are produced under operation conditions, raising the local pH and increasing the thermodynamic potential for the HER (Fig. 2B). Such pH drifting at the cathode shortens the potential gap between cation reduction and the HER, promoting the electroreduction of cations. The resulting impurity layers on the electrode surface can hinder the mass transfer of water molecules during operation and cause instability, as demonstrated by Amal and coworkers.[16] In their report, a manganese doped nickel/nickel oxide (Mn-doped Ni/NiO) electrocatalyst exhibited a highly stable HER performance in phosphate buffer (PB) solution (pH = 7) with minor fluctuation (<10%) over 48 hours. However, when PB solution was replaced with natural seawater (pH = ~8.2), the quantity of experimental H_2 production deviated from theoretical values with merely 70% faradaic efficiency after 7 hours (Fig. 2C), meaning that the competing reactions had consumed 30% of the total charge. Repeated electrolysis revealed severe activity loss in three runs (Fig. 2D), which was attributed to the formation of a white layer (Fig. 2E) consisting of Na, Ca, and Mg salts, as indicated by X-ray photoelectron spectroscopy (XPS) results.

Moreover, during operation, the local pH drifts can create an acidic environment at the anode and an alkaline environment at the cathode. Such pH drift is directly related to the electrode potential and reaction rate.[15] As an alkaline condition is established at the cathode, the formation of insoluble precipitates, such as MgO, $Mg(OH)_2$, and $Ca(OH)_2$, is promoted at the electrode surface (red region in Fig. 2B).

Nevertheless, such surface blockage is not limited to the cathode; it is extended to the anode and porous diaphragm (membrane). For PEMWE, metal ions can occupy the sites for proton exchange in the membrane to increase the charge transfer resistance and reduce the reaction rate.[17] Likewise, Cl^- ions may lower the exchange efficiency of the anion exchange membrane in AEMWE.[18] Moreover, natural seawater often contains various concentrations of biomaterials (bacteria and microbes), which can cause precipitation and adhesion on the surface of the electrode and membrane, further hindering charge transfer and water diffusion.

3.3. HER competing reactions

For water electrolysis, the competing oxygen reduction reaction (ORR) often occurs at the cathode due to O_2 crossover from the anode side.[21] The ORR has a much higher thermodynamic potential than the HER, which would result in additional energy consumption and lower HER efficiency. Seawater naturally contains dissolved oxygen (Table 1) that further decreases the efficiency.

The reduction of Cl_2/ClO^- (reactions (5) and (6)) is another competing reaction at the cathode during seawater electrolysis. Similar to the ORR, these species can migrate from the anode side, across the diaphragm or membrane, and compete with H_2O molecules for active sites.

Other minor competing reactions, including $B(OH)_3$ and CO_2 reduction, are not as notable and are rarely mentioned in the literature for seawater electrolysis. Their thermodynamic reduction potential values are lower than the HER (*e.g.*, −0.48 V for $B(OH)_3/BH_4^-$ −0.53 V for CO_2/CO);[8,22] thus, their electrochemical reduction occurs at high HER overpotentials. For seawater electrolysis performed at a large voltage, such side effects are inevitable. Noticeable effects, in addition to the faradaic efficiency loss from these side reactions, may be accumulated from their reduction products such as CO during long-term electrolysis. Jaramillo's group demonstrated that in an electrolyte containing dissolved CO_2, the HER activity trend of transition metals shifted due to the surface adsorbed CO species.[23] In particular, the Pt catalyst was deactivated as the CO species formed on its surface.

3.4. Electrocatalyst poisoning and corrosion

The above-mentioned surface blockage can be considered as a form of surface poisoning. Active site poisoning, one of the primary causes of electrocatalyst deactivation in many electrocatalytic processes, is another form. Impurities (ions and molecules) in electrolytes often interact with the active sites and block the adsorption of reactants. Sometimes, such interaction is strong enough to dissociate the electrocatalysts, causing surface corrosion and the release of metal ions from the electrocatalysts into the electrolyte. For seawater electrolysis, ions such as Cl^-, Mg^{2+}, and Ca^{2+} are most likely responsible for the catalyst poisoning and corrosion at the anode and cathode.

The existence of cations in the electrolyte can alter the OER performance dramatically.[24] This is because cations can interact with lattice oxygen and/or substitute some cations on the electrocatalysts. However, no comprehensive study on the impact of Ca^{2+} and Mg^{2+} on OER activity is available. For some noble metal surfaces, cations can be deposited under potential, resulting in decreased intrinsic activity.[25]

Currently, Pt is regarded as the best HER electrocatalyst, and Pt-based materials are widely used in commercial water electrolyzers. However, the abundant Cl^- ions in seawater can bind strongly with Pt atoms to result in the dissolution of the catalyst.[26] Multiple reports confirmed the complete deactivation of commercial 20% Pt/C within 5 h during seawater electrolysis.[27,28] Similar dissolution behaviour is also known in some state-of-the-art OER electrocatalysts, like IrO_2.[29] Some non-precious metal-based catalysts are even more vulnerable than the noble metals. Wang *et al.* recently showed that CoP, MoP, and MoS_2 catalysts could be corroded at both open-circuit potential (OCP) and HER potential in an acidic electrolyte to release metal ions, and CoP showed a high dissolution ratio of ~25% at OCP.[30] Moysiadou *et al.* provided a comprehensive stability analysis of the common transition-metal based OER catalysts, including CoO_x, $CoFeO_x$, NiO_x, $NiFeO_x$, and $CoFeNiO_x$. Both CoO_x and $CoFeO_x$ suffered from dissolution at the initial OER stage, and all catalysts exhibited compositional changes at the OER condition, releasing Fe ions into the electrolyte.[31]

 This journal is © The Royal Society of Chemistry 2021

Published on 16 August 2021. Downloaded by Hong Kong Polytechnic University on 9/9/2021 5:39:47 AM.

Corrosion also occurs at the current collector. Typically, an electrode of the water electrolyzer is configured as a composite of a metallic current collector (often Ti, steel, and carbon) coated with an electrocatalyst layer. Since carbon supports can be easily corroded at high potential,[32] metallic supports are usually preferred. However, the electrooxidation of the metallic current collectors can sometimes contaminate the electrolyte by releasing metal ions into electrolytes.[33] Moreover, the formation of an oxide layer on the current collector can increase the charge transfer resistance.[34]

3.5. Physical damage

Apart from the issues related to the unique composition of seawater, physical issues such as catalyst detachment, particle agglomeration, phase transition, bubble formation, and membrane degradation[5,33,35,36] have also been widely identified as challenges toward long-term stable water electrolysis (Fig. 3): These are directly caused by the harsh conditions of industrial water electrolysis such as the high reaction rate (*i.e.*, high current density), excessive potential, and electrolyte flow.

The detachment of active materials from the electrode results in poor conductivity between the catalysts and the current collectors (supporting electrodes). The enlarged particle size during electrolysis decreases the total population of the active sites exposed to the surface. Structural transition of catalysts often leads to deterioration from active phases to inactive phases. Last but not least, the inevitable formation of H_2 and O_2 bubbles on the electrode surface creates a bubble curtain that makes the catalytic surface temporarily inaccessible by electrolyte until the bubble is detached. Such a masking effect by bubble formation was reported to cause 5 to 10% energy loss.[37]

4. Current countermeasures

The current research effort focuses mainly on two aspects, electrocatalyst design and electrode engineering, for minimizing performance loss during long-term operation and extending the lifetime of electrolyzers. The former intends to reduce side reactions (mostly chloride oxidation reaction), electrocatalyst corrosion, and poisoning by rational design of active sites. The latter aims to address the problem of surface blockage, adhesion, and physical damages such as detachment. Innovative cell designs have also been investigated recently.

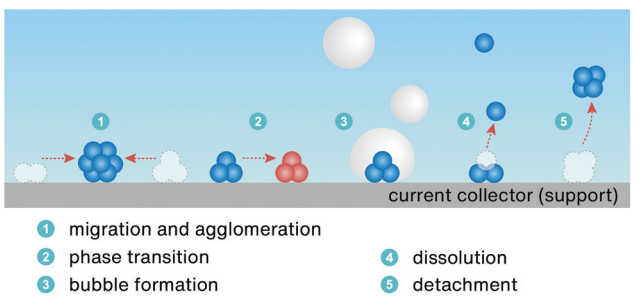

Fig. 3 Schematic overview showing common causes of electrocatalyst deactivation during electrocatalysis.

4.1. Electrocatalyst design

Selective anodic reaction. The problems associated with Cl_2 production within the electrolyzers can be eliminated by increasing the anodic selectivity towards the OER over chloride oxidation. Electrochemically speaking, the OER needs to be performed at a desired current density at a potential lower than the chloride oxidation requirement. The OER has a lower thermodynamic overpotential than the chloride oxidation in the entire pH range of 0–14, and the difference between the two anodic reactions depends on the pH (Fig. 4A). The maximum difference is close to 480 mV in alkaline media, while it drops to ~130 mV at pH = 0. With this guidance, two strategies (Fig. 4B), the lowering of the OER overpotential and the lifting of the chloride oxidation overpotential, are adopted.

The tuning of the pH of seawater toward alkaline to maintain the most significant potential difference is the most straightforward method.[19] Under alkaline conditions, the OER can be catalyzed at the desired reaction rate without initiating chloride oxidation (Fig. 4C). Currently, NiFe oxyhydroxide materials are among the best OER catalysts.[38,39] Using NiFe oxyhydroxide-based electrocatalysts, Dionigi *et al.* showed a nearly 100% OER selectivity at a benchmarking current density of 10 mA cm^{-2} even with Cl^- in the electrolyte.[19] Recently, Yang and co-workers demonstrated a low overpotential of 258 mV for 1 A cm^{-2} using a NiFe oxyhydroxide-anchored NiFe alloy nanowire system that can remain stable for 120 h.[40] Since there are ample examples of alkaline OER electrocatalysts with low overpotential in the literature,[41] we will not discuss them further.

Another method is to increase the overpotential of chloride oxidation. This helps suppress the rate of chloride oxidation even when its thermodynamic potential is reached. Unlike the alkaline OER with a limiting potential window of up to 480 mV, this method can be applied for the entire pH range, thus allowing more room for high current density seawater electrolysis. Yet, this method remains challenging since the OER active sites are usually active for chloride oxidation as well.[42,43] For this approach, Co- and Ru-based electrocatalysts are the most promising candidates.[44] Common strategies, from surface doping to electrolyte tuning, all focus on reducing the surface adsorption of Cl^- ions.[45,46] Cheng *et al.* described a selective OER (530 mV for 10 mA cm^{-2}, 99.94% selectivity) in unbuffered near-neutral pH seawater using a CoFe layered double hydroxide (LDH).[47] They argued that the synergistic action between the LDH and ions in seawater improved the selectivity, but the fundamental mechanistic understanding was lacking. In another report, the $Pb_2Ru_2O_{7-x}$ electrocatalyst showed ~99% and ~68% OER selectivity at pH = 13 and 7, respectively, in a Cl^--containing electrolyte, a result that was attributed to the tuning of the Ru sites and oxygen vacancies.[44]

Published on 16 August 2021. Downloaded by Hong Kong Polytechnic University on 9/9/2021 5:39:47 AM.

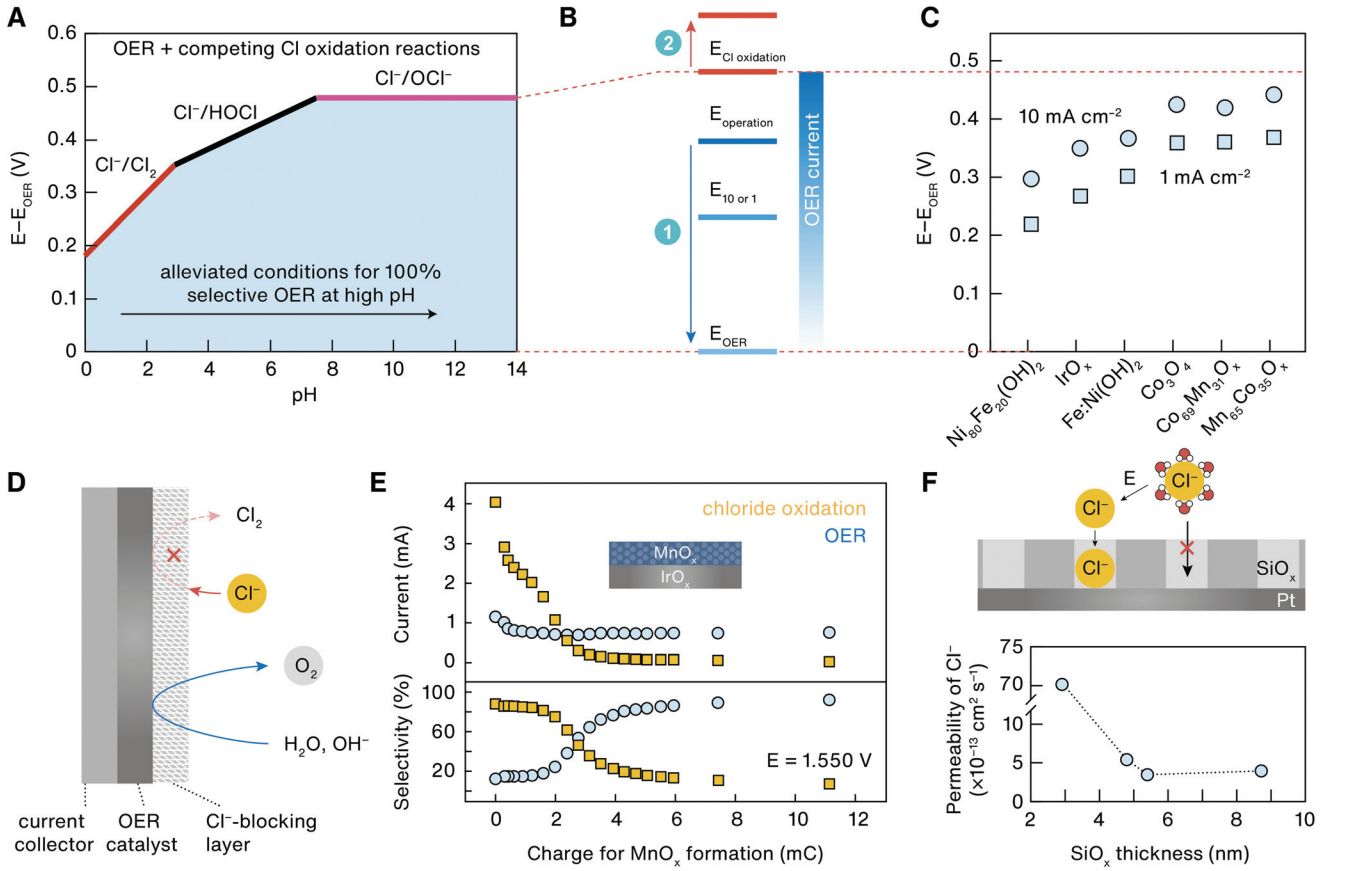

Fig. 4 (A) Predicted kinetic overpotential allowance as a function of pH for 100% OER selectivity over chloride oxidation. Reproduced with permission,[19] 2016 Wiley-VCH. (B) Two design strategies to improve OER selectivity at high current density: 1. Lowering the OER overpotential; 2. Increasing the chloride oxidation overpotential. (C) Experimental OER overpotentials of some state-of-the-art catalysts in alkaline electrolytes at the current density of 1 mA cm^{-2} (square) and 10 mA cm^{-2} (round). Reproduced with permission,[7] 2020 Springer Nature. (D) Engaging a Cl^--blocking layer on the catalyst to increase the chloride oxidation overpotential. (E) Current density (top) and selectivity (bottom) of OER (round) and chloride oxidation (square) on a MnO_x-coated IrO_x electrocatalyst in an acidic electrolyte. The charge for MnO_x formation indicates the thickness of the MnO_x overlayer: a higher charge leads to a thicker layer. Reproduced with permission,[50] 2018 American Chemical Society. (F) Illustration of additional energy requirement for Cl^- ion dehydration (top) and permeability of Cl^- ions in SiO_x overlayers with an increasing thickness (bottom). The bottom panel is adopted with permission,[51] 2021 American Chemical Society.

The decrease of the local concentration of Cl^- ions near the anode *via* electrocatalyst design is more commonly adopted, and a typical way to do so is by building a Cl^--blocking layer on the catalyst surface (Fig. 4D).[48,49] Such a layer slows the kinetics of chloride oxidation and reduces possible corrosion caused by Cl^- ions. A recent study conducted by Koper and co-workers under acidic conditions showed that MnO_x could act as a permeable overlayer (~5–20 nm) on the IrO_x catalyst to interrupt the transport of Cl^- ions to the active sites, resulting in an OER selectivity improvement from 14 to >93% (Fig. 4E).[50] Likewise, Esposito *et al.* demonstrated a similar Cl^- ion blocking functionality using the SiO_x overlayer on Pt in both acidic and unbuffered pH-neutral seawater electrolysis (Fig. 4F).[51] Such selectivity was explained by the extra energy needed to dehydrate the surrounding H_2O molecules of Cl^- ions to penetrate the size-selective pores of the SiO_x overlayer.

Engaging an overlayer is not a must to block Cl^- ions, as suggested by Dai and co-workers who introduced a NiS_x underlayer for NiFe OER catalysts.[52] The *in situ* formed sulfate anions during alkaline seawater electrolysis generated a cation-selective polyatomic anion-rich environment on the anode surface which repulsed Cl^- ions. Such an electrode demonstrated ~100% OER selectivity and remarkable stability over 1000 h of electrolysis at 400 mA cm^{-2}. A similar S-doped NiFe oxyhydroxide catalyst reported by Yu *et al.* in 2020 also accomplished high OER selectivity at 500 mA cm^{-2}.[38]

Poisoning/corrosion-resistance HER catalyst. Pt, currently the best HER catalyst, suffers from surface poisoning by cations and Cl^--induced corrosion in long-term electrolysis. Great effort has been made to improve the stability of Pt-based catalysts[53] and to develop non-noble metal-based electrocatalysts that can operate in the whole pH range.[28,54] Surface engineering of HER catalysts, including doping[16] and vacancy engineering,[55] is frequently adopted to reduce cation (Ca^{2+} and Mg^{2+}) poisoning. Since this topic of Pt poisoning and its

 This journal is © The Royal Society of Chemistry 2021

Published on 16 August 2021. Downloaded by Hong Kong Polytechnic University on 9/9/2021 5:39:47 AM.

prevention has been well-reviewed in recent literature,[5,56,57] we will not discuss it in detail here.

Transition metal sulfide/phosphide/nitride and hydroxides are the most promising systems for the acidic and alkaline HER, respectively.[54,58–62] These materials are considered better candidates over Pt for the HER in seawater due to their resistance to Cl^--induced corrosion.[63] Despite the initial dissolution of the electrocatalysts in the electrolyte, their long-term stability is considerably higher than that of the noble metal catalysts.[5,64] Ledendecker *et al.* suggested that, for metal carbides, sulfides, and phosphides as HER catalysts, the initial contact with the electrolyte and the instant dissolution were critical for the overall stability during long-term electrolysis.[64] Engaging pre-treatments to remove the dangling bonds, defects, and surface oxides was suggested to improve the overall stability.

4.2. Electrode engineering

Surface protection. Applying a surface protection layer (or passivation layer) on top of the active materials (Fig. 5A) is a common strategy to minimize the impact of corrosion/dissolution/detachment. As previously discussed, NiFe oxyhydroxides are among the most promising OER catalysts. However, the FeOOH species can be dissolved in alkaline solutions during the OER, causing its deactivation.[65,66] Obata *et al.* showed that a CeO_x layer, which allowed OH^- and O_2 diffusion while preventing Fe species from releasing into the electrolyte, could solve such problems (Fig. 5B).[67] Compared with the unprotected catalyst, the CeO_x-coated catalyst showed a minor degradation over 96 h of electrolysis (Fig. 5C). Moreover, the layer inhibited the undesired Cl^- ions from approaching the surface and improved the anodic selectivity. In the literature, the coating of the catalyst with a carbon shell is the most popular strategy, and it has been proven effective in preventing particle migration and dissolution.[27,28] However, the existence of the surface layer inevitably reduces the mass transport efficiency and blocks some active sites, sacrificing activity for stability. One typical example is the aforementioned SiO_x layer over the Pt electrocatalyst for a selective OER.[51] Despite its high selectivity, the current density of the SiO_x-protected Pt electrocatalyst dropped by 90% compared with that of the unprotected one. The trade-off between activity and stability can be fine-tuned by adjusting the thickness of the SiO_x layer. As they pointed out, an optimized thickness of 4.8 nm delivered the best stability with a moderate activity for seawater electrolysis.

Enhancement of catalyst–support interaction. The disadvantage of the surface protection layer can be avoided by engaging an underlayer that can firmly anchor the electrocatalyst, directly exposing the catalytically active sites to the electrolyte. By doing so, the intense interaction between the supporting layer and the active materials can help reducing catalyst detachment and particle agglomeration (Fig. 5D).

Such a strategy is widely adopted for the emerging single-atom (SA) electrocatalysts. Despite their extraordinary activity for water electrolysis, the isolated atomic metal sites tend to aggregate and form particles with lower surface energy. The use of oxide/MXene/doped carbon supports with strong interaction with the metal atoms can significantly improve the durability of SA active sites.[68,69] For example, Zang *et al.* presented an electrocatalyst of atomically dispersed Ni sites with triple nitrogen coordination for the HER and delivered negligible current attenuation during 14 hours of seawater electrolysis.[58] Thanks to the strong Ni–N interaction, the coordination environment of Ni remained stable even after 5000 cycles with minor activity loss (Fig. 5E).

For the more conventional nanoparticle catalysts, the importance of enhancing the catalyst–support interaction has been widely recognized.[74–76] In 2019, Ren and co-workers described a composite OER catalyst made of NiFeN nanoparticles decorated on NiMoN nanorods (Fig. 5F).[70] The strong electronic interaction between NiFeN and NiMoN was shown to prevent detachment and corrosion, which enabled a current density of 1 A cm^{-2} at an overpotential of 398 mV with high stability over 100 h in alkaline seawater. In a similar fashion, Sun *et al.* built the NiCo structure directly on the MXene surface (Fig. 5G) and demonstrated a high HER stability over 140 h at a current density of 500 mA cm^{-2}.[71]

Increasing bubble escape rate. During the water electrolysis operation, the adhesion of H_2 and O_2 bubbles on the electrode surface temporary blocks the active sites, resulting in a sudden ohmic drop and disrupted mass transfer (Fig. 5H).[77,78] In a recent review article, Angulo *et al.* discussed in detail the formation and impact of bubbles within the electrochemical cell.[79] Unlike planar supporting electrodes used in the laboratory, industrial water electrolysis often involves a porous support/current collector to allocate active materials as much as possible. The micro tunnels further complicate the diffusion path of the generated gas.[80] Therefore, quick diffusion and release of gas bubbles are of vital importance to seawater electrolysis.

The key to resolving these bubble issues is to create a surface that naturally promotes water adsorption and facilitates gas release (Fig. 5I). Two approaches have been proven effective: the chemical modification of catalyst composite and the construction of a 3-dimensional (3D) electrocatalyst structure. Li *et al.* compared the OER activities of $NiFe(OH)_x$ before and after phosphorylation and showed that the OER overpotential could be dramatically reduced by phosphorylation (Fig. 5I).[72] In another report, Kou *et al.* demonstrated the power of 3D-printing in building optimized 3D supporting structures that could facilitate rapid bubble transport and release (Fig. 5J).[73] The carbon-doped NiO grown on periodic porous 3D printed Ni (3DPNi) electrodes delivered 1 A cm^{-2} of HER and OER at overpotentials of 245 and 425 mV, respectively, which outperformed the commercial nickel foam. Also, the 3D structure delivered a stable large current density of 850 mA cm^{-2} at 2.2 V and 80 °C for at least 16 h, which is superior to many industrial electrolyzers under similar conditions.

Published on 16 August 2021. Downloaded by Hong Kong Polytechnic University on 9/9/2021 5:39:47 AM.

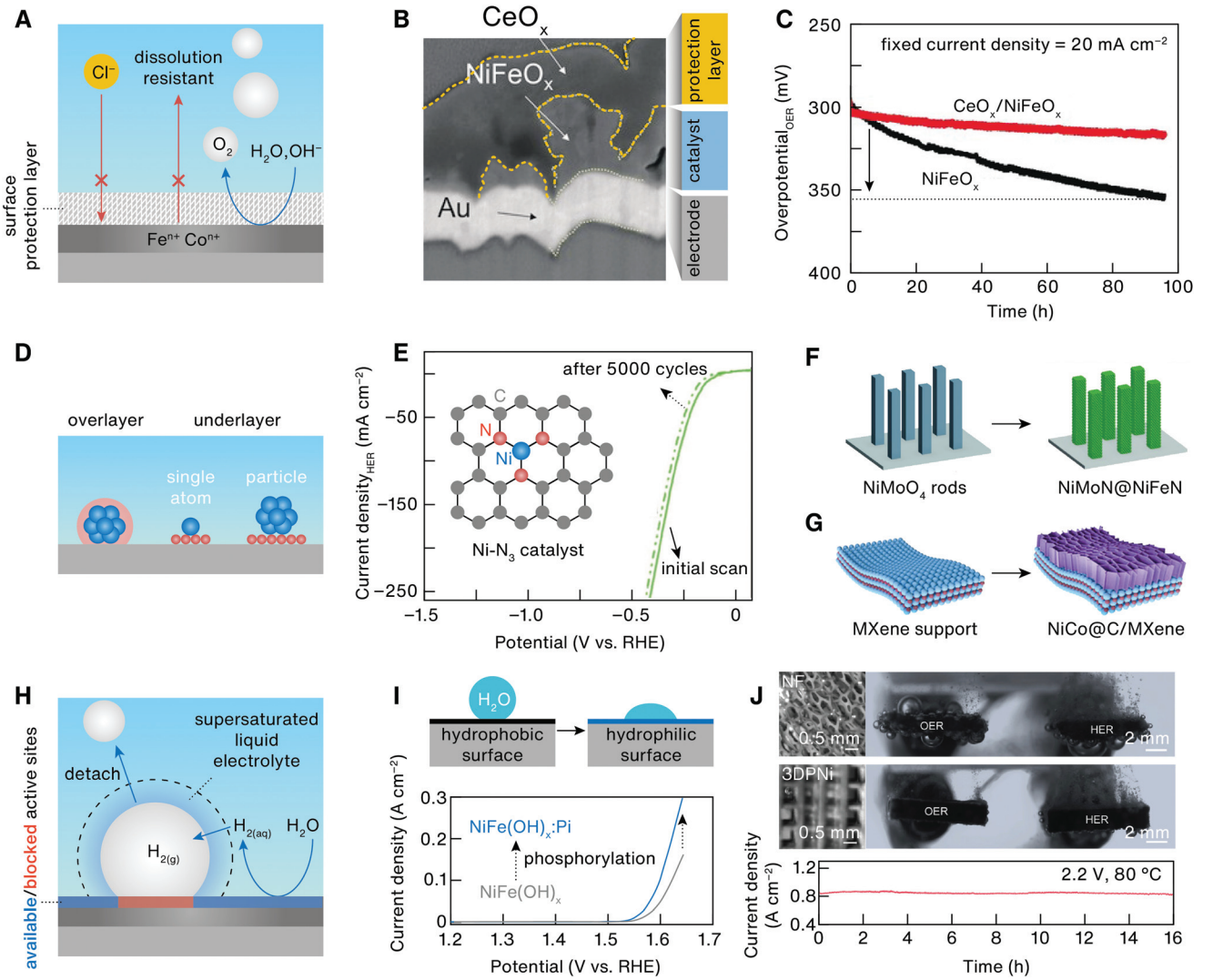

Fig. 5 (A) Engaging a surface protection layer over catalysts to prevent dissolution and Cl^--induced corrosion. (B) Cross-sectional scanning electron microscopic image of CeO_x-coated $NiFeO_x$. (C) OER overpotential drift of protected and unprotected electrocatalysts during 96 h of electrolysis at a current density of 20 mA cm^{-2}. Panels B and C are reproduced with permission,[67] 2018 Wiley-VCH. (D) Two strategies of minimizing catalyst dissolution: surface overlayer and catalyst underlayer. (E) HER polarization curves of the Ni–N3 SA electrocatalyst before and after 5000 cycles. Inset: Structural illustration of the electrocatalyst. Reproduced with permission,[58] 2020 Wiley-VCH. (F) NiFeN electrocatalyst on the NiMoN support. Reproduced with permission,[70] 2019 Springer Nature. (G) NiCo@C electrocatalyst on the MXene support. Reproduced with permission,[71] 2021 Springer Nature. (H) Mechanism of bubble formation during gas evolution reactions. The red surface indicates blocked active sites by a bubble, while blue represents unblocked sites. (I) Chemical modification of the catalyst surface from hydrophobic to hydrophilic to improve water adsorption (top) and an example showing the improved OER activity after phosphorylation of catalyst (bottom). The bottom panel is reproduced with permission,[72] 2017 American Chemical Society. (J) Reaction photos (top) comparing the bubble release from catalyst-coated commercial nickel foam (NF, top) and 3D-printed nickel structure (3DPNi, bottom). The bottom panel shows the chronoamperogram of the 3DPNi-supported catalyst at a cell voltage of 2.2 V and temperature of 80 °C for 16 h. Reproduced with permission,[73] 2020 Wiley-VCH.

4.3. Cell design

So far, our discussion has focused on the electrode design to adopt the existing cell configurations of AWE and AEMWE for direct seawater electrolysis. Recently, innovative efforts have also been made to change the cell configuration specifically to fit seawater electrolysis. In 2020, Strasser and co-workers demonstrated a concept of asymmetric electrolyte, where neutral seawater was fed directly at the cathode in a single pass while a pure KOH electrolyte was circulated at the anode.[81] Such cell design significantly reduced the Cl^- concentration at the anodic side, thus, guaranteeing high selectivity towards the OER. One can also replace the kinetically slow OER process by other oxidation reactions to bypass the Cl-based side reactions. In 2021, Qiu's group demonstrated a hybrid seawater electrolyzer involving hydrazine oxidation (−0.33 V *vs.* RHE for N_2H_4/N_2) at the anode. This cell could be operated at low voltages of 0.7–1.0 V with high stability over

 This journal is © The Royal Society of Chemistry 2021

Published on 16 August 2021. Downloaded by Hong Kong Polytechnic University on 9/9/2021 5:39:47 AM.

140 h at 500 mA cm^{-2}. Likewise, the membrane was also engineered to achieve ion selectivity in seawater electrolysis.[82] All of these new designs aimed to reduce the impact of seawater composites on catalyst deactivation and cell degradation.

5. Conclusion and outlook

In this review, we have identified the general causes of performance decline during long-term seawater electrolysis, including chloride oxidation, surface blockage, competing reactions, surface poisoning, corrosion, detachment, agglomeration, and bubble formation. Some are triggered by the composition of seawater (especially Cl^-, Mg^{2+}, and Ca^{2+}), and others are commonly shared by other water electrolysis technologies. We have further outlined the current effort to address these problems, from electrocatalyst design to electrode engineering and cell design.

As a clean and sustainable approach of producing hydrogen, the research on electrochemical water electrolysis has rapidly progressed in the last few decades. Yet, its wide industrial application is much slower than the thriving academic research due to high cost. Using seawater directly as the electrolyte, instead of pure water, represents an economically more attractive route towards cheaper hydrogen fuel. As the price of electricity drops, we expect that hydrogen produced using seawater electrolysis will become more competitive than other methods, especially the conventional carbon-based ones. It will also promote the adoption of hydrogen energy in remote regions.

However, direct seawater electrolysis is still in a preliminary stage, even compared with other electrolysis techniques such as AWE and PEMWE. Most recent studies focus on the activity and selectivity of the catalysts, while the demonstration of long-term performance stability remains an option in the literature. Since the goal of such techniques is a stable and affordable hydrogen production, we expect more studies to be carried out on the performance stability of many active materials to fairly evaluate their real potential in industrial seawater electrolysis.

In this regard, standard criteria need to be set up for the benchmarking of activity and stability between different systems, including the electrolyte composite, electrolysis time, and current density. Currently, some materials are only tested under simulated conditions (*e.g.*, NaCl solution), and the potential influence of co-existing cations and other impurities is unknown/unstudied. A consensus on the testing parameters (electrolysis time, current density, electrolyte composition) needs to be reached among the research community to further improve material screening and commercialization of seawater electrolyzers.

Finally, we expect more works related to the structural engineering of electrodes and electrochemical cells to bring new opportunities to fundamental research and industrial applications of seawater electrolysis. With the suitable active materials identified, the subsequent engineering problems, such as fixing the active materials on the electrode and minimizing the catalyst loss during operation, will be critical for real-life operation. As discussed in this review, an overall consideration from catalyst development to electrode engineering and cell design is needed to realize cheap hydrogen production from practically unlimited seawater.

Conflicts of interest

The authors declare no competing interests.

Acknowledgements

The authors acknowledge the support from the Innovation and Technology Commission of Hong Kong and the Hong Kong Polytechnic University (grant number Q-CDA3). KYW also acknowledges the support from the Patrick S.C. Poon endowed professorship.

References

1 I. Staffell, D. Scamman, A. Velazquez Abad, P. Balcombe, P. E. Dodds, P. Ekins, N. Shah and K. R. Ward, *Energy Environ. Sci.*, 2019, **12**, 463–491.
2 J. Kibsgaard and I. Chorkendorff, *Nat. Energy*, 2019, **4**, 430–433.
3 O. Schmidt, A. Gambhir, I. Staffell, A. Hawkes, J. Nelson and S. Few, *Int. J. Hydrogen Energy*, 2017, **42**, 30470–30492.
4 G. A. Lindquist, Q. Xu, S. Z. Oener and S. W. Boettcher, *Joule*, 2020, **4**, 2549–2561.
5 H. Jin, B. Ruqia, Y. Park, H. J. Kim, H. S. Oh, S. I. Choi and K. Lee, *Adv. Energy Mater.*, 2020, **11**, 2003188.
6 I. Halevy and A. Bachan, *Science*, 2017, **355**, 1069–1071.
7 W. M. Tong, M. Forster, F. Dionigi, S. Dresp, R. S. Erami, P. Strasser, A. J. Cowan and P. Farras, *Nat. Energy*, 2020, **5**, 367–377.
8 S. Dresp, F. Dionigi, M. Klingenhof and P. Strasser, *ACS Energy Lett.*, 2019, **4**, 933–942.
9 R. d'Amore-Domenech, Ó. Santiago and T. J. Leo, *Renewable Sustainable Energy Rev.*, 2020, **133**, 110166.
10 S. Khatun, H. Hirani and P. Roy, *J. Mater. Chem. A*, 2021, **9**, 74–86.
11 A. Maljusch, O. Conradi, S. Hoch, M. Blug and W. Schuhmann, *Anal. Chem.*, 2016, **88**, 7597–7602.
12 F. J. Millero, R. Feistel, D. G. Wright and T. J. McDougall, *Deep Sea Res., Part I*, 2008, **55**, 50–72.
13 J. G. Vos, A. Venugopal, W. A. Smith and M. T. M. Koper, *J. Catal.*, 2020, **389**, 99–110.
14 E. L. Liening, in *Corrosion: Environments and Industries*, ed. J. S. D. Cramer and B. S. Covino, ASM International Handbook Committee, 2006, vol. 13C.
15 I. Katsounaros, J. C. Meier, S. O. Klemm, A. A. Topalov, P. U. Biedermann, M. Auinger and K. J. J. Mayrhofer, *Electrochem. Commun.*, 2011, **13**, 634–637.

Published on 16 August 2021. Downloaded by Hong Kong Polytechnic University on 9/9/2021 5:39:47 AM.

16 X. Lu, J. Pan, E. Lovell, T. H. Tan, Y. H. Ng and R. Amal, *Energy Environ. Sci.*, 2018, **11**, 1898–1910.
17 B. L. Kienitz, H. Baskaran and T. A. Zawodzinski, *Electrochim. Acta*, 2009, **54**, 1671–1679.
18 S. Dresp, F. Dionigi, S. Loos, J. Ferreira de Araujo, C. Spöri, M. Gliech, H. Dau and P. Strasser, *Adv. Energy Mater.*, 2018, **8**, 1800338.
19 F. Dionigi, T. Reier, Z. Pawolek, M. Gliech and P. Strasser, *ChemSusChem*, 2016, **9**, 962–972.
20 K. A. Persson, B. Waldwick, P. Lazic and G. Ceder, *Phys. Rev. B: Condens. Matter Mater. Phys.*, 2012, **85**, 235438.
21 P. Trinke, B. Bensmann and R. Hanke-Rauschenbach, *Electrochem. Commun.*, 2017, **82**, 98–102.
22 A. Goyal, G. Marcandalli, V. A. Mints and M. T. M. Koper, *J. Am. Chem. Soc.*, 2020, **142**, 4154–4161.
23 E. R. Cave, C. Shi, K. P. Kuhl, T. Hatsukade, D. N. Abram, C. Hahn, K. Chan and T. F. Jaramillo, *ACS Catal.*, 2018, **8**, 3035–3040.
24 C. Yang, G. Rousse, K. Louise Svane, P. E. Pearce, A. M. Abakumov, M. Deschamps, G. Cibin, A. V. Chadwick, D. A. Dalla Corte, H. Anton Hansen, T. Vegge, J. M. Tarascon and A. Grimaud, *Nat. Commun.*, 2020, **11**, 1378.
25 Q. Feng, X. Z. Yuan, G. Liu, B. Wei, Z. Zhang, H. Li and H. Wang, *J. Power Sources*, 2017, **366**, 33–55.
26 S. Geiger, S. Cherevko and K. J. J. Mayrhofer, *Electrochim. Acta*, 2015, **179**, 24–31.
27 X. Wu, S. Zhou, Z. Wang, J. Liu, W. Pei, P. Yang, J. Zhao and J. Qiu, *Adv. Energy Mater.*, 2019, **9**, 1901333.
28 Y.-Y. Ma, C.-X. Wu, X.-J. Feng, H.-Q. Tan, L.-K. Yan, Y. Liu, Z.-H. Kang, E.-B. Wang and Y.-G. Li, *Energy Environ. Sci.*, 2017, **10**, 788–798.
29 X. Tan, J. Shen, N. Semagina and M. Secanell, *J. Catal.*, 2019, **371**, 57–70.
30 Z. Wang, Y.-R. Zheng, J. Montoya, D. Hochfilzer, A. Cao, J. Kibsgaard, I. Chorkendorff and J. K. Nørskov, *ACS Energy Lett.*, 2021, **6**, 2268–2274.
31 A. Moysiadou and X. Hu, *J. Mater. Chem. A*, 2019, **7**, 25865–25877.
32 L. Castanheira, W. O. Silva, F. H. B. Lima, A. Crisci, L. Dubau and F. Maillard, *ACS Catal.*, 2015, **5**, 2184–2194.
33 C. Rakousky, U. Reimer, K. Wippermann, M. Carmo, W. Lueke and D. Stolten, *J. Power Sources*, 2016, **326**, 120–128.
34 S. M. Hoseinieh, F. Ashrafizadeh and M. H. Maddahi, *J. Electrochem. Soc.*, 2010, **157**, E50.
35 W. Zheng, M. Liu and L. Y. S. Lee, *ACS Catal.*, 2019, **10**, 81–92.
36 L. Liu and A. Corma, *Nat. Rev. Chem.*, 2021, **5**, 256–276.
37 G. F. Swiegers, R. N. L. Terrett, G. Tsekouras, T. Tsuzuki, R. J. Pace and R. Stranger, *Sustainable Energy Fuels*, 2021, **5**, 1280–1310.
38 L. Yu, L. Wu, B. McElhenny, S. Song, D. Luo, F. Zhang, Y. Yu, S. Chen and Z. Ren, *Energy Environ. Sci.*, 2020, **13**, 3439–3446.
39 S. Duan, Z. Liu, H. Zhuo, T. Wang, J. Liu, L. Wang, J. Liang, J. Han, Y. Huang and Q. Li, *Nanoscale*, 2020, **12**, 21743–21749.
40 C. Liang, P. Zou, A. Nairan, Y. Zhang, J. Liu, K. Liu, S. Hu, F. Kang, H. J. Fan and C. Yang, *Energy Environ. Sci.*, 2020, **13**, 86–95.
41 N. T. Suen, S. F. Hung, Q. Quan, N. Zhang, Y. J. Xu and H. M. Chen, *Chem. Soc. Rev.*, 2017, **46**, 337–365.
42 S. Trasatti, *Electrochim. Acta*, 1984, **29**, 1503–1512.
43 J. G. Vos, Z. Liu, F. D. Speck, N. Perini, W. Fu, S. Cherevko and M. T. M. Koper, *ACS Catal.*, 2019, **9**, 8561–8574.
44 K. S. Exner, *ChemElectroChem*, 2019, **6**, 3401–3409.
45 H. J. Song, H. Yoon, B. Ju, D.-Y. Lee and D.-W. Kim, *ACS Catal.*, 2019, **10**, 702–709.
46 F. H. Zhang, L. Yu, L. B. Wu, D. Luo and Z. F. Ren, *Trends Chem.*, 2021, **3**, 485–498.
47 F. Cheng, X. Feng, X. Chen, W. Lin, J. Rong and W. Yang, *Electrochim. Acta*, 2017, **251**, 336–343.
48 W. H. Hung, B. Y. Xue, T. M. Lin, S. Y. Lu and I. Y. Tsao, *Mater. Today Energy*, 2021, **19**, 100575.
49 A. R. Jadhav, A. Kumar, J. Lee, T. Yang, S. Na, J. Lee, Y. Luo, X. Liu, Y. Hwang, Y. Liu and H. Lee, *J. Mater. Chem. A*, 2020, **8**, 24501–24514.
50 J. G. Vos, T. A. Wezendonk, A. W. Jeremiasse and M. T. M. Koper, *J. Am. Chem. Soc.*, 2018, **140**, 10270–10281.
51 A. A. Bhardwaj, J. G. Vos, M. E. S. Beatty, A. F. Baxter, M. T. M. Koper, N. Y. Yip and D. V. Esposito, *ACS Catal.*, 2021, **11**, 1316–1330.
52 Y. Kuang, M. J. Kenney, Y. Meng, W. H. Hung, Y. Liu, J. E. Huang, R. Prasanna, P. Li, Y. Li, L. Wang, M. C. Lin, M. D. McGehee, X. Sun and H. Dai, *Proc. Natl. Acad. Sci. U. S. A.*, 2019, **116**, 6624–6629.
53 J. Zheng, Y. Zhao, H. Xi and C. Li, *RSC Adv.*, 2018, **8**, 9423–9429.
54 Z. Wang, W. Xu, K. Yu, Y. Feng and Z. Zhu, *Nanoscale*, 2020, **12**, 6176–6187.
55 G. Zhou, Z. Guo, Y. Shan, S. Wu, J. Zhang, K. Yan, L. Liu, P. K. Chu and X. Wu, *Nano Energy*, 2019, **55**, 42–48.
56 J. Zhu, L. Hu, P. Zhao, L. Y. S. Lee and K. Y. Wong, *Chem. Rev.*, 2020, **120**, 851–918.
57 C. Wang, H. Shang, L. Jin, H. Xu and Y. Du, *Nanoscale*, 2021, **13**, 7897–7912.
58 W. Zang, T. Sun, T. Yang, S. Xi, M. Waqar, Z. Kou, Z. Lyu, Y. P. Feng, J. Wang and S. J. Pennycook, *Adv. Mater.*, 2021, **33**, e2003846.
59 C. Wang, M. Zhu, Z. Cao, P. Zhu, Y. Cao, X. Xu, C. Xu and Z. Yin, *Appl. Catal., B*, 2021, **291**, 120071.
60 J. Mohammed-Ibrahim and H. Moussab, *Mater. Sci. Energy Technol.*, 2020, **3**, 780–807.
61 L. Wu, L. Yu, F. Zhang, B. McElhenny, D. Luo, A. Karim, S. Chen and Z. Ren, *Adv. Funct. Mater.*, 2020, **31**, 2006484.
62 H. Jin, X. Liu, A. Vasileff, Y. Jiao, Y. Zhao, Y. Zheng and S. Z. Qiao, *ACS Nano*, 2018, **12**, 12761–12769.
63 L. Yu, L. Wu, S. Song, B. McElhenny, F. Zhang, S. Chen and Z. Ren, *ACS Energy Lett.*, 2020, **5**, 2681–2689.
64 M. Ledendecker, J. S. Mondschein, O. Kasian, S. Geiger, D. Gohl, M. Schalenbach, A. Zeradjanin, S. Cherevko,

 This journal is © The Royal Society of Chemistry 2021

Published on 16 August 2021. Downloaded by Hong Kong Polytechnic University on 9/9/2021 5:39:47 AM.

R. E. Schaak and K. Mayrhofer, *Angew. Chem., Int. Ed.*, 2017, **56**, 9767–9771.
65 S. Zou, M. S. Burke, M. G. Kast, J. Fan, N. Danilovic and S. W. Boettcher, *Chem. Mater.*, 2015, **27**, 8011–8020.
66 F. D. Speck, K. E. Dettelbach, R. S. Sherbo, D. A. Salvatore, A. Huang and C. P. Berlinguette, *Chem*, 2017, **2**, 590–597.
67 K. Obata and K. Takanabe, *Angew. Chem., Int. Ed.*, 2018, **57**, 1616–1620.
68 J. Yang, W. Li, D. Wang and Y. Li, *Adv. Mater.*, 2020, **32**, e2003300.
69 L. Xiu, W. Pei, S. Zhou, Z. Wang, P. Yang, J. Zhao and J. Qiu, *Adv. Funct. Mater.*, 2020, **30**, 1910028.
70 L. Yu, Q. Zhu, S. Song, B. McElhenny, D. Wang, C. Wu, Z. Qin, J. Bao, Y. Yu, S. Chen and Z. Ren, *Nat. Commun.*, 2019, **10**, 5106.
71 F. Sun, J. Qin, Z. Wang, M. Yu, X. Wu, X. Sun and J. Qiu, *Nat. Commun.*, 2021, **12**, 4182.
72 Y. Li and C. Zhao, *ACS Catal.*, 2017, **7**, 2535–2541.
73 T. Kou, S. Wang, R. Shi, T. Zhang, S. Chiovoloni, J. Q. Lu, W. Chen, M. A. Worsley, B. C. Wood, S. E. Baker, E. B. Duoss, R. Wu, C. Zhu and Y. Li, *Adv. Energy Mater.*, 2020, **10**, 2002955.
74 I. Jimenez-Morales, S. Cavaliere, D. Jones and J. Roziere, *Phys. Chem. Chem. Phys.*, 2018, **20**, 8765–8772.
75 X. Wu, B. Feng, W. Li, Y. Niu, Y. Yu, S. Lu, C. Zhong, P. Liu, Z. Tian, L. Chen, W. Hu and C. M. Li, *Nano Energy*, 2019, **62**, 117–126.
76 Y. Liu, X. Hu, B. Huang and Z. Xie, *ACS Sustainable Chem. Eng.*, 2019, **7**, 18835–18843.
77 D. Zhang and K. Zeng, *Ind. Eng. Chem. Res.*, 2012, **51**, 13825–13832.
78 A. R. Zeradjanin, P. Narangoda, I. Spanos, J. Masa and R. Schlögl, *Curr. Opin. Electrochem.*, 2021, **30**, 100797.
79 A. Angulo, P. van der Linde, H. Gardeniers, M. Modestino and D. Fernández Rivas, *Joule*, 2020, **4**, 555–579.
80 T. Kadyk, D. Bruce and M. Eikerling, *Sci. Rep.*, 2016, **6**, 38780.
81 S. Dresp, T. Ngo Thanh, M. Klingenhof, S. Brückner, P. Hauke and P. Strasser, *Energy Environ. Sci.*, 2020, **13**, 1725–1729.
82 L. Shi, R. Rossi, M. Son, D. M. Hall, M. A. Hickner, C. A. Gorski and B. E. Logan, *Energy Environ. Sci.*, 2020, **13**, 3138–3148.